

Mudbanks of the Southwest Coast of India IV: Mud Viscoelastic Properties

Feng Jiang[†] and Ashish J. Mehta[‡]

[†]Moffatt & Nichol, Engineers
2809 Boston Street
Baltimore, MD 21224, U.S.A.

[‡]Coastal and Oceanographic
Engineering Department
University of Florida
Gainesville, FL 32611, U.S.A.

ABSTRACT



JIANG, F. and MEHTA, A.J., 1995. Mudbanks of the southwest coast of India IV: Mud viscoelastic properties. *Journal of Coastal Research*, 11(3), 918-926. Fort Lauderdale (Florida), ISSN 0749-0208.

A small-strain rheological model has been developed to characterize the complex equivalent viscosity in the equation of mud motion due to water waves. The dynamic viscosity and the shear moduli of elasticity in this model are determined from creep and dynamic shear tests in a controlled-stress rheometer, and their dependence on the forcing stress amplitude, frequency and the solids volume fraction is examined. For a comparative evaluation of mud rheology, the model has been applied to mud samples obtained from the southwest coast of India, Lake Okeechobee in Florida and Mobile Bay in Alabama, and to an aqueous clay mixture. In each case within the measured stress amplitude range, the viscoelastic coefficients are found to depend significantly on the forcing frequency, for a given solids volume fraction. The India mud is found to be the most viscous of those tested. This high viscosity results in very high rates of wave energy dissipation off the coast of Kerala during the monsoon season.

ADDITIONAL INDEX WORDS: *Creep compliance, mudbanks, rheometer, wave energy, yield stress.*

INTRODUCTION

Subaqueous mud composed of fine-grained sediment can substantially attenuate water waves as they pass over mudbanks and in the process also modulate the wave energy spectrum. Off the coast of Kerala in southwest India, MATHEW *et al.* (1994) report wave energy dissipation on the order of 90% over a comparatively short distance of about 1 km in an area where a mudbank occurs during nearly every monsoon season. From their work on mudbanks off the coast of Surinam, WELLS and KEMP (1986) found not only 88% loss of the incoming wave energy over a distance of 11 km, but also observed that the typical, wide-band oceanic wave spectrum changed to one approaching that for a solitary wave. JIANG and MEHTA (1992) recorded the occurrence of a surf beat-like, low frequency forced wave in the bottom mud resulting from the interaction between the forcing wind-wave frequencies.

Given the significance of wave energy dissipation due to bottom mud, including selective attenuation of the forcing frequencies and their interaction, the equation of mud motion in which mud is conventionally represented as an incom-

pressible continuum must accurately account for its rheological constitutive properties. To that end, previous observations by, *e.g.*, MAA (1986), CHOU (1989), and JIANG (1993), suggest that the commonly used Kelvin or Voigt viscoelastic representation may be overly simplistic; *i.e.*, it does not consistently predict the rate of wave energy dissipation with sufficient accuracy, especially at comparatively low frequencies of marine interest. Here therefore a more general model is developed to characterize mud rheology relevant to wave-mud interaction studies. We shall begin by briefly stating the theoretical and experimental bases of the approach; then present results for a mud sample obtained off Alleppey in Kerala, India (FAAS, 1995), lake mud, estuarine mud and an aqueous clay mixture.

CONSTITUTIVE EQUATION

For an incompressible continuous medium, the equation of motion is:

$$\rho \frac{Du_i}{Dt} = -\rho g \delta_{3i} - \frac{\partial p}{\partial x_i} + \frac{\partial T_{ji}}{\partial x_j} \quad (1)$$

where $\rho(x_i, t)$ = density, $u_i(x_i, t)$ = velocity components, g = acceleration due to gravity, $p(x_i, t)$ =

mean normal pressure, $T_{ji}(x_i, t)$ = spherical components of the external surface stresses, t = time, x_i = spatial coordinate, subscript i denotes direction, and subscripts i and j denote directions in conjunction with the composite subscript ji , which implies a second order tensor. Thus, j is the direction normal to the surface and i is the stress direction. Furthermore, δ_{ji} = kronecker delta, such that for $j = i$, $\delta_{ji} = 1$, and for $j \neq i$, $\delta_{ji} = 0$. Further development of Eq. 1 depends on the choice of the constitutive equation for the rheology. Considering E_{ji} to represent small strain, the general constitutive equation for a linear viscoelastic medium is

$$\sum_{r=0}^M p_r \frac{\partial^r T_{ji}}{\partial t^r} = \sum_{s=0}^N q_s \frac{\partial^s E_{ji}}{\partial t^s} \quad (2)$$

where r and s denote orders of partial differentiation, p_r and q_s are coefficients related to the chosen viscoelastic model, and M and N are the specified maximum differential orders of the chosen model. Under cyclic loading at an angular frequency ω , we consider harmonic representations

$$T_{ji} = T^0 \exp(-i\omega t) \quad (3)$$

$$E_{ji} = E^0 \exp[-i(\omega t - \delta)] \quad (4)$$

where T^0 and E^0 are amplitudes of T_{ji} and E_{ji} , respectively, δ is the corresponding phase shift, and $i = (-1)^{1/2}$. Then, by substituting Equations 3 and 4 into Equation 2 the relation between the stress and the strain becomes

$$\frac{T_{ji}}{E_{ji}} = \frac{\sum_{s=0}^N q_s (-i\omega)^s}{\sum_{r=0}^M p_r (-i\omega)^r} \quad (5)$$

and the corresponding relation between the stress and the rate of strain is

$$\frac{T_{ji}}{\dot{E}_{ji}} = \frac{\sum_{s=0}^N q_s (-i\omega)^s}{\sum_{r=0}^M p_r (-i\omega)^{r+1}} = \mu^* \quad (6)$$

where the dot denotes time-derivative, and $\mu^* = \mu' + i\mu''$ is referred to as the complex equivalent viscosity, in which μ' = real part, or the dynamic viscosity, and μ'' = imaginary part, called the second viscosity, representing the elastic component

(BARNES *et al.*, 1989). Noting that $\dot{E}_{ji} = \partial u_i / \partial x_j$, the equation of motion then becomes

$$\rho \frac{Du_i}{Dt} = -\rho g \delta_{3i} - \frac{\partial p}{\partial x} + \mu^* \frac{\partial^2 u_i}{\partial x_j \partial x_j} \quad (7)$$

Thus, the solution of Equation 7 is contingent upon the form of μ^* . For example, from Equation 6, for a Newtonian fluid:

$$\mu' = \mu \quad \mu'' = 0 \quad (8)$$

where μ is the fluid viscosity. Likewise, for a Hookean elastic material:

$$\mu' = 0 \quad \mu'' = \frac{G}{\omega} \quad (9)$$

where G is the shear modulus of elasticity.

We will next consider two basic viscoelastic models—Voigt and Maxwell. The former is a linear combination of a Hookean elastic element and a Newtonian fluid element in parallel, while the latter consists of the same two elements in series (BARNES *et al.*, 1989). Thus, for the Voigt model:

$$\mu' = \mu \quad \mu'' = \frac{G}{\omega} \quad (10)$$

and for the Maxwell model:

$$\mu' = \frac{2G \left(\frac{G}{\mu} \right)}{\omega^2 + \left(\frac{G}{\mu} \right)^2} \quad \mu'' = \frac{2G\omega}{\omega^2 + \left(\frac{G}{\mu} \right)^2} \quad (11)$$

The Maxwell model essentially represents a fluid since it dissipates an instantaneously applied stress at a rate that depends on the characteristic relaxation time, μ/G . However, stress relaxation tests on marine muds at typical *in situ* densities indicate that a residual stress generally remains; hence, the Maxwell model is not a suitable general choice for mud rheology, even though it appears to be approximately descriptive of mud in the fluidized state (MAA, 1986; WILLIAMS and WILLIAMS, 1992). On the other hand, rheometric data on the time-variation of strain in creep tests on mud samples do not seem to conform to the Voigt model consistently (JIANG, 1993). Finally, at forcing frequencies ($f = \omega/2\pi$) in the vicinity of 1.5 Hz and less, the use of Voigt description for bottom mud rheology in hydrodynamic models apparently yields water wave attenuation rates that differ from those measured in the laboratory set-

ting (JIANG, 1993). Thus, recognizing the need to improve the rheological description, without however resorting to the development of a complex model that would require extensive characterization measurements, a three-parameter model obtained by a suitable combination of the Voigt and Maxwell elements is considered here.

Mathematically, the simplest choice beyond the Voigt/Maxwell representations would be to select the 0th and the 1st order time- derivatives of stress and strain in Equation 5 (MALVERN, 1969). The mechanical analog shown in Figure 1, also referred to as the standard linear solid, is one possible configuration (KOLSKY, 1992), which has been used successfully to model the consolidation behavior of soils (KEEDWELL, 1984). Given the relative similarity between that problem and wave-mud interaction, we will assume the applicability of the standard linear solid model without formally establishing its uniqueness as a tool for the description of the physical behavior sought and then discuss the consequences. For convenience of further development, we will select the symbols τ and γ to represent T_{ji} and E_{ji} , respectively. Thus, we state

$$\tau + \alpha_1 \dot{\tau} = \beta_0 \gamma + \beta_1 \dot{\gamma} \tag{12}$$

where, based on the force balance for the analog of Figure 1, the coefficients, $\alpha_1 = \mu/(G_1 + G_2)$, $\beta_0 = 2G_1 G_2 / (G_1 + G_2)$ and $\beta_1 = 2\mu G_1 / (G_1 + G_2)$. Alternatively, from Equations 3, 4 and 6,

$$\begin{aligned} \mu' &= \frac{2G_1 \left(\frac{G_1}{\mu} \right)}{\left(\frac{G_1 + G_2}{\mu} \right)^2 + \omega^2}; \\ \mu'' &= \frac{2 \left(\frac{G_1}{\omega} \right) \left[\frac{(G_1 + G_2) G_2}{\mu^2} + \omega^2 \right]}{\left(\frac{G_1 + G_2}{\mu} \right)^2 + \omega^2} \end{aligned} \tag{13}$$

It thus remains to measure μ , G_1 and G_2 in order to calculate μ' and μ'' , hence $\mu^* = \tau/\dot{\gamma}$. Note that in the limit, setting $G_2/G_1 = 0$ in Eq. 12 or 13 yields the Voigt model, *i.e.*, $\tau = 2G_2\gamma + 2\mu\dot{\gamma}$, while setting $G_2 = 0$ implies the Maxwell behavior, *i.e.*, $\tau + (\mu/G_1)\dot{\tau} = 2\mu\dot{\gamma}$.

RHEOMETRY

The evaluation of the viscoelastic coefficients was done through creep and dynamic, or oscilla-

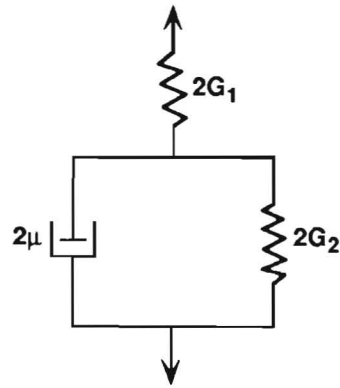


Figure 1. Mechanical analog of the three-parameter viscoelastic model, also called a standard linear solid (KOLSKY, 1992).

tory shear, tests in a Carri-Med CSL controlled-stress rheometer (JIANG, 1993). The loading and unloading stages of the creep test on a sample are represented as

$$\tau = \begin{cases} \tau_0, & \text{for } 0 \leq t \leq t_c \\ 0, & \text{for } t_c < t \end{cases} \tag{14}$$

where τ_0 is an applied constant stress. In the dynamic test the stress input and strain output functions corresponding to Equations 3 and 4 are,

$$\tau = \tau^0 \exp(-i\omega t) \tag{15}$$

$$\gamma = \gamma^0 \exp[-i(\omega t - \delta)] \tag{16}$$

where τ^0 and γ^0 are the amplitudes of τ and γ , respectively, and δ is the phase shift. In the case of a purely elastic response $\delta = 0$, while $\delta = \pi/2$ corresponds to a purely viscous behavior. Thus, in general, for a viscoelastic material, $0 < \delta < \pi/2$. For the model of Equation 12 (or 13), the coefficients are found to be (JIANG, 1993):

$$\mu = \frac{\tau^0}{\gamma^0} \frac{\omega}{\sin \delta (\omega^2 + T_c^2)} \tag{17}$$

$$G_1 = \frac{\tau^0}{\gamma^0} \frac{\omega \cos \delta - T_c \sin \delta}{\omega \cos \delta - T_c \sin \delta} \tag{18}$$

$$G_2 = \frac{\tau^0}{\gamma^0} \frac{\omega T_c}{\sin \delta (\omega^2 + T_c^2)} \tag{19}$$

where the time constant (units of inverse time), $T_c = \beta_0/\beta_1$, such that $T_c^{-1} = \mu/G_2$ is a characteristic measure of the viscous retardation of an otherwise instantaneous elastic response of the element of shear modulus G_2 .

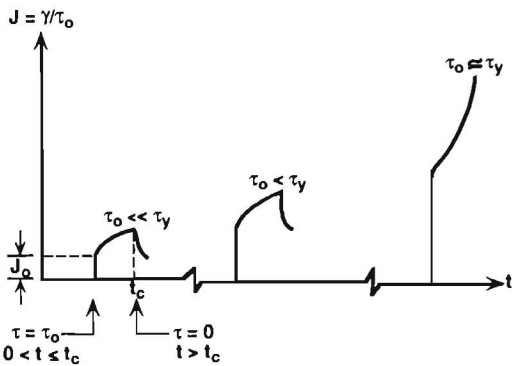


Figure 2. Schematic plot of creep-compliance versus time for three relative magnitudes of the applied stress.

To qualitatively illustrate the characteristics of a creep test in Figure 2, the time-dependence of the creep-compliance, $J = \gamma/\tau_0$, is schematized for three increasing values of τ_0 . While the first two tests signify viscoelastic responses, the third test corresponds approximately to incipient thixotropic yield, hence $\tau_0 \approx \tau_y$, the yield stress, which is equal to the upper limit of τ_0 at which an elastic response can be measured. As indicated by the nature of the curves, the variation of the initial, instantaneous compliance, J_0 , a measure of elastic response with the applied stress is contingent upon the state of the material. For Equation 12 (or 13), J_0 represents the initial condition which must be specified to simulate the creep (time-variation of strain) curve, since the initial instantaneous elastic response is not described by that model.

Some characteristics of the muds tested are given in Table 1, including the median dispersed particle size, solids volume fraction, ϕ , and the principal constituents. The volume fractions of the KI and OK muds correspond to those of the samples obtained *in situ*, while the ϕ values of the other two were varied by dilution. In the creep

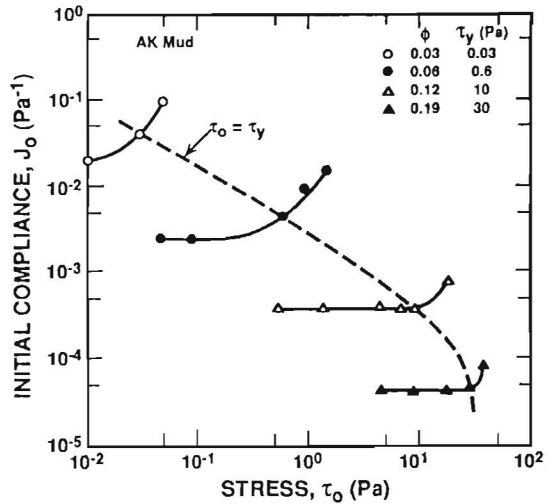


Figure 3. Initial compliance versus applied stress for AK mud.

tests, τ_0 was varied from 0.01 up to 40 Pa, whereas in the dynamic tests, τ^0 ranged from 0.3 up to 7 Pa, and the forcing frequency was varied from 0.02 to 4 Hz.

An example of the variation of J_0 with τ_0 for the AK (attapulgitite + kaolinite) mud is shown in Figure 3. The curve for each ϕ has been divided approximately by the dashed line representing the yield condition. At stresses lower than τ_y , J_0 is observed to typically increase gradually with τ_0 , with the rate of increase decreasing with increasing ϕ . In fact, with the possible exception of the curve for $\phi = 0.03$, the dependence of J_0 on τ_0 is weak, which suggests a practically linear viscoelastic response from this perspective. Once yield commences, J_0 increases rapidly with τ_0 in accordance with the depiction in Figure 2. Comparing the curves for increasing ϕ , a dramatic corresponding rise in τ_y becomes apparent, as described in Figure 4. This rise can be considered to be

Table 1. Mud characteristics.

Type	Median Size (μm)	ϕ	Principal Constituents
Kerala, India mud (KI)	2	0.12	Montmorillonite, kaolinite, illite, gibbsite, organic matter (5%)*
Okeechobee mud (OK)	9	0.11	Kaolinite, sepiolite, montmorillonite, organic matter (40%)
Mobile Bay mud (MB)	15	0.07 to 0.17	Clayey silt of undetermined composition, sand
Attapulgitite + kaolinite (AK)	1	0.03 to 0.19	Attapulgitite (50%), kaolinite (50%)

*By weight

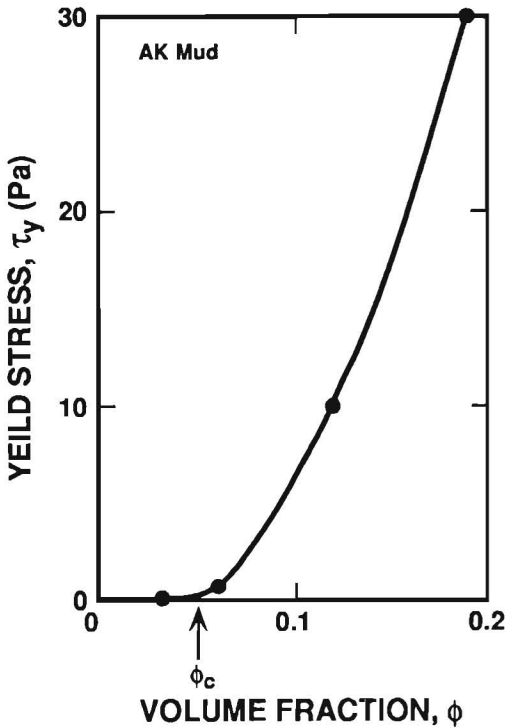


Figure 4. Yield stress versus solids volume fraction for AK mud.

associated with the development of a space-filling particulate network structure as ϕ exceeds a "critical" value, ϕ_c . The data suggest this value to be in the vicinity of 0.05, which is comparable with ϕ_c for other muds (JAMES *et al.*, 1988). The occurrence of such a threshold value in turn provides a possible explanation for the nature of the J_0 versus τ_0 curve for $\phi = 0.03$ in Figure 3, which shows no clearly identifiable value of τ_y , since space-filling was evidently incomplete in that case.

For $\tau_0 < \tau_y$, we will illustrate the calculation of μ , G_1 and G_2 using the data of the OK (Okeechobee) mud, which was typical in terms of the data trends, despite the high organic content. Figure 5 shows a typical γ - t response curve during a creep test. With reference to Equation 12 as the basis for the chosen model for simulating this response, terms involving derivatives of γ higher than the first have been included elsewhere in describing the behavior of other materials, *e.g.*, for the appropriate degree of accuracy in treating the rheology of polymers (BARNES *et al.*, 1989). However,

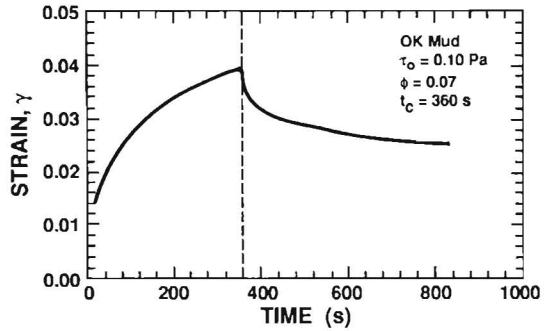


Figure 5. A typical example of the time-variation of strain during a creep test. Data from a test using OK mud.

as observed from the illustrative case of Figure 6 for the OK mud, $\dot{\gamma}$ and $\ddot{\gamma}$ are essentially uncorrelated. This independence lends a heuristic justification for ignoring higher, second order derivatives when dealing with muds.

In Figure 7, $\dot{\gamma}$ is plotted against γ for the stress loading and unloading phases corresponding to the test shown in Figure 5. Reasonably linear relationships are observed except at the low strain end of the loading phase and the high strain end of the unloading phase. As outlined elsewhere (JIANG, 1993), these deviations from linearity are likely to be due to the influence of instrument inertia on the time-strain variation. Furthermore, the fact that the two slopes are nearly parallel elsewhere implies that the time constant T_c , the slope of the linear segment, is not measurably influenced by the stress, τ_0 . This observation is generalized by the data of Figure 8, where T_c is seen to increase with the volume fraction, ϕ , apparently due to the rapid increase in bed rigidity

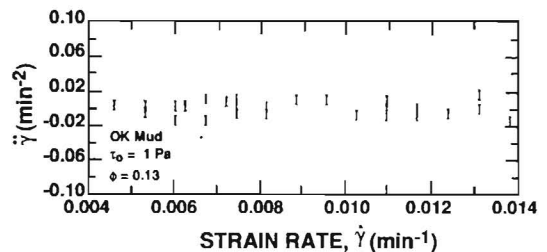


Figure 6. A typical example of variation of the rate of strain rate with strain rate. Data from a creep test using OK mud.

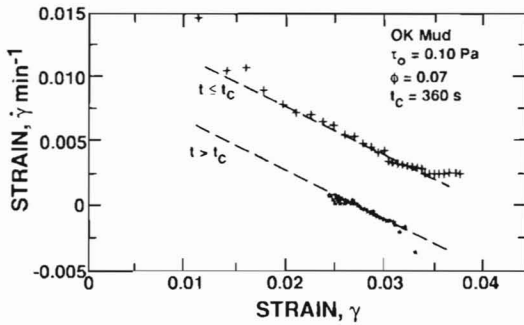


Figure 7. Variation of the rate of strain with strain in the creep test corresponding to Figure 5.

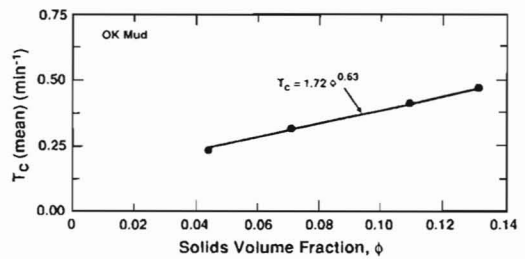


Figure 9. Dependence of the stress-mean time constant, T_c , on the solids volume fraction for OK mud.

with ϕ . In Figure 9, the stress-mean value of T_c has been plotted against ϕ , recognizing the limitation introduced by the averaging process over ranges of τ_0 that are different for each ϕ . Thus, one obtains the following approximate relation

$$T_c = \alpha_2 \phi^{\beta_2} \quad (20)$$

where $\alpha_2 = 1.72$ and $\beta_2 = 0.63$, given T_c in min^{-1} .

Under the assumption that α_2 and β_2 in Equation 20 are characteristic constants, Equations 17, 18 and 19 can be used to determine the viscoelastic parameters, provided γ^0 and δ are measured for a given τ^0 and forcing frequency through dynamic tests.

VISCOELASTIC PARAMETERS

Parameters μ , G_1 and G_2 for AK mud ($\phi = 0.12$) are plotted against τ^0 in Figures 10a,b,c at three illustrative forcing frequencies. Note, the generally weak dependence of the parameters on the stress in comparison with frequency. In Figures 11a,b,c this frequency dependence is apparent

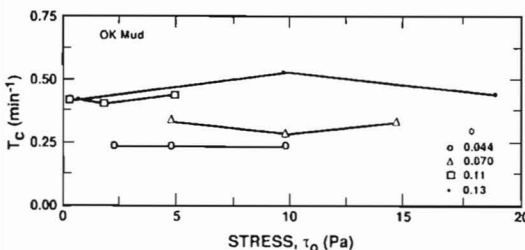


Figure 8. Dependence of the time constant, T_c , on the stress and the solids volume fraction for OK mud.

from data at three representative values of the applied stress. Observe that the increase in G_1 with f signifies a corresponding approach to a Voigt-like response with increasing frequency.

When mud is fluidized by water wave motion, *in situ* measurements in the laboratory flume using a miniature shearometer have indicated that the shear modulus decreases and approaches zero in the course of hours (WILLIAMS and WILLIAMS, 1992). This change in the state of mud from a viscoelastic to a viscous medium has a measurable influence on its dissipative properties, despite the fact that the typical values of the characteristic shear modulus, G_2 , are comparatively low to moderate, on the order of 10^3 Pa and less (*cf.* 4×10^{10} Pa for cast iron). This influence of the state of mud on energy dissipation is illustrated in an indirect way in Figure 12, in which a hydrodynamic model that incorporates the three-parameter model to describe mud rheology was used to calculate the dependence of the water wave attenuation coefficient, k_i , on frequency (JIANG, 1993). The coefficient, k_i , is defined by the relation, $a_x = a_0 \exp(-k_i x)$, where x ($= x_i$) is the longitudinal distance coordinate, a_0 = wave amplitude at $x = 0$, and a_x = amplitude at a distance x . The selected water depth was 16 cm and mud depth 12 cm. Curve A was obtained by using $\mu = 10$ Pa·s, $G_1 = 200$ Pa and $G_2 = 30$ Pa. In addition to the significant dependence of attenuation on frequency, the suggestion of resonance corresponding to the peak value of k_i is found to be governed by the mud depth normalized by the wave-induced mud boundary layer thickness (JIANG, 1993). At frequencies that are high relative to the resonance frequency, the wave motion hardly reaches the bottom, while at low frequencies the shear rate (hence energy dissipation) in the mud layer

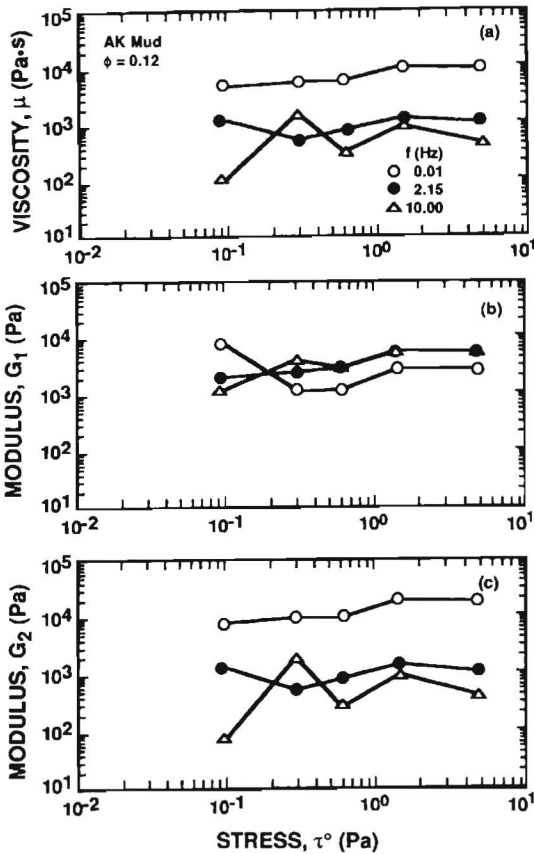


Figure 10. Variation of the viscoelastic parameters with stress at three frequencies for AK mud: a) Plots for μ , b) Plots for G_1 , and c) Plots for G_2 .

is comparatively small due to the relatively uniform vertical distribution of the horizontal wave velocity. As a result in both cases the attenuation coefficient is low. Elsewhere (JIANG, 1993) it is shown that this modeling approach shows a good agreement with attenuation coefficients measured in a laboratory flume using the AK mud. Curve B corresponds to $\mu = 10 \text{ Pa}\cdot\text{s}$, $G_1 \rightarrow \infty$ and $G_2 = 0$, *i.e.*, a purely viscous medium, *e.g.* mud in the fluidized state, for which the degree of dissipation is increased in comparison with that for the viscoelastic mud. Thus, in general, even a small degree of elasticity can measurably modulate the energy dissipation process. In any event, the dependence of k , on the boundary layer, hence wave frequency, typically modulates the input spec-

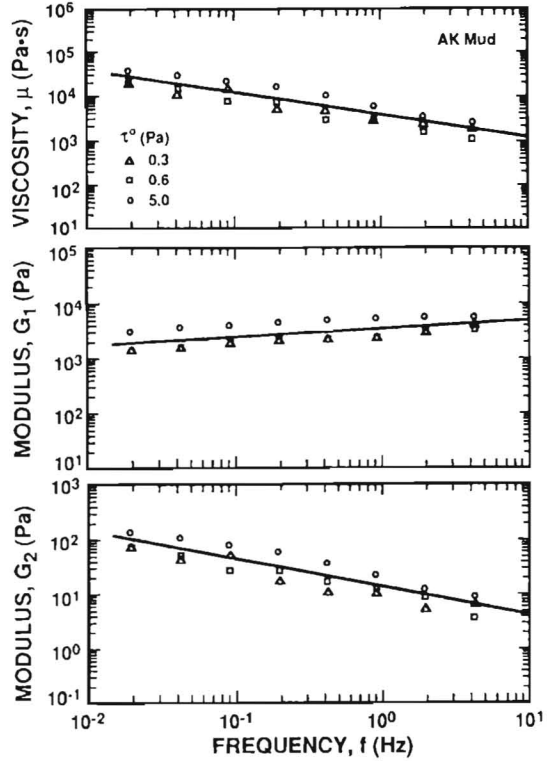


Figure 11. Variation of the viscoelastic parameters with frequency for AK mud: a) Data for μ , b) Data for G_1 , and c) Data for G_2 .

trum especially a wide-band one, due to selective damping.

The best-fit straight lines in Figure 11a,b,c can be generally expressed as

$$\mu, G_1, G_2 = \exp(\epsilon) \cdot f^\Delta \quad (21)$$

for which values of ϵ and Δ are given in Table 2 for the four muds, all of which showed trends compatible with Equation 21 (JIANG, 1993; JIANG and MEHTA, 1993). In general, all the viscoelastic parameters are observed to depend on frequency in different degrees, which in turn implies that the three-parameter model is essentially operational, as opposed to one in which the characterizing parameters are true constants, *i.e.*, independent of frequency. It is uncertain at this time if such a general model can be developed without considering the thermodynamic effects that may be inherently important when the mud sample is loaded at different frequencies. Such is the case

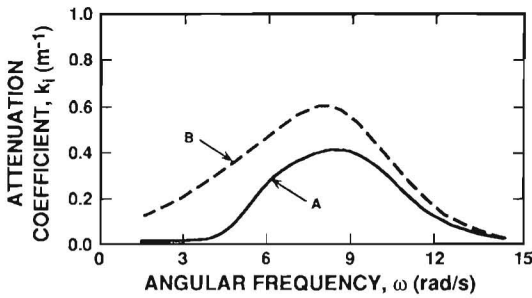


Figure 12. Theoretically calculated wave attenuation coefficient as a function of angular frequency. Curve A is with the three parameter model, while curve B corresponds to the viscous fluid approximation of the same model.

because of the likelihood that over the frequency range chosen in this study at comparatively low frequencies, the energy dissipation process tends to be isothermal; while with increasing frequency, the process becomes increasingly adiabatic (KRIZEK, 1971; SCHREUDER *et al.*, 1986).

The influence of the solids volume fraction on viscoelasticity is described for the MB (Mobile Bay) mud in Figure 13, in which the magnitude of the complex equivalent viscosity, $|\mu^*| = (\mu'^2 + \mu''^2)^{1/2}$, is plotted against frequency for three mud samples of different ϕ values. Observe the consistent decrease in $|\mu^*|$ with increasing f , and its increase with ϕ . For an illustrative inter-comparison of the viscoelastic properties of the MB mud of different solids volume fractions, as well as the other muds, values of μ and G_2 at the representative frequency of 0.1 Hz are given in Table 3. The additional contribution from G_1 to the constitutive behavior may be ignored for this simple comparative purpose. The KI (Kerala, India) mud is seen to be the most viscous and rigid of those tested. Its high viscosity undoubtedly correlates with the very high rates of wave energy dissipation

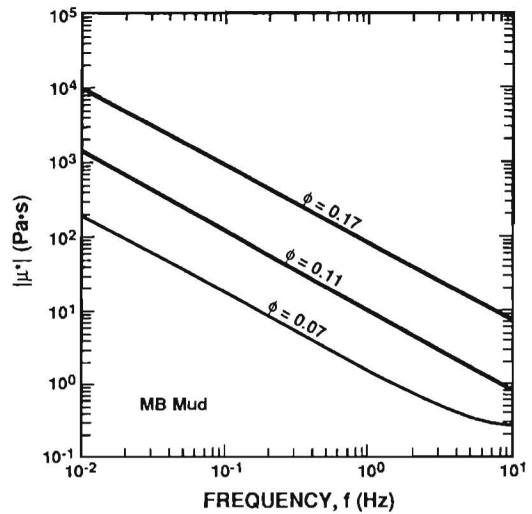


Figure 13. Variation of the magnitude of the complex equivalent viscosity with frequency and solids volume fraction for MB mud.

off the coast of Kerala during the monsoon season (MATHEW, 1992). The OK mud is relatively low in viscosity and rigidity, consistent with its high organic content. The silty MB mud has low viscosity as well as low rigidity at $\phi = 0.07$; however, the viscosity increases rapidly with increasing solids volume fraction. Finally, the AK mud is observed to be both highly viscous and comparatively rigid, mainly due to the thixotropic attapulgitic.

The variation of viscosity of the mud with its density as well as the rate of shear is believed to have a controlling influence on the seasonal cross-shore motion of the mudbanks of Kerala. As noted by FAAS (1995), the seasonal variation in the wave climate brings about wave-induced changes in mud rheology as well as rates of mud shear. These

Table 2. Coefficients of Eq. 21 for KI, OK, MB and AK muds, for selected values of ϕ .

Mud	ϕ	G_1 (Pa)		G_2 (Pa)		μ (Pa·sec)	
		ϵ	Δ	ϵ	Δ	ϵ	Δ
KI	0.12	9.160	0.257	3.843	-0.405	9.292	-0.405
OK	0.11	5.548	0.127	0.318	-0.687	5.290	-0.687
MB	0.07	3.659	-0.030	-1.439	-0.975	3.165	-0.975
MB	0.11	6.352	0.075	2.139	-0.745	6.695	-0.745
MB	0.17	8.274	0.108	-3.864	-0.696	8.374	-0.696
AK	0.12	8.049	0.114	2.604	-0.490	8.222	-0.490

Table 3. Parameters μ and G_2 for the muds at $f = 0.1$ Hz.

Mud	ϕ	μ (Pa·sec)	G_2 (Pa)
KI	0.12	2.76×10^4	1.19×10^2
OK	0.11	9.65×10^2	1.78×10^0
MB	0.07	2.24×10^2	2.43×10^{-1}
MB	0.11	4.49×10^3	1.06×10^1
MB	0.17	2.15×10^4	1.04×10^1
AK	0.12	1.15×10^4	4.18×10^1

changes cumulatively determine the position of the mudbank relative to the shoreline. During monsoon the mudbank occurs close to the shore where it causes the waves to damp, while during fair weather the relatively low density mud slides offshore into deeper waters in the absence of high waves (MATHEW *et al.*, 1994).

CONCLUDING COMMENTS

Substantial further work remains to elucidate the true rheological behavior of muds. The operational model proposed here is semi-empirical, and its applicability is theoretically limited to stresses lower than the yield stress. Nevertheless, the use of this model using the KI mud has been shown to lead to satisfactory simulation of the damped wave spectrum measured off the town of Alleppey in Kerala (JIANG, 1993). However in future efforts of this nature, it will be desirable to account for the yield behavior in an explicit way, since in the prototype environment the imposed stresses under episodic conditions surely exceed the threshold for yield. The canonical Maxwell model with distributed relaxation processes is likely to be the preferred candidate for post-yield simulation, given the fluid-like state of mud under strong and sustained wave-induced motion.

ACKNOWLEDGEMENT

Support from WES contract DACW39-90-K-0010 is acknowledged.

LITERATURE CITED

- BARNES, H.A.; HUTTON, J.F., and WALTERS, K., 1989. *An Introduction to Rheology*. Amsterdam: Elsevier, 208p.
- CHOU, H.T. 1989. Rheological Response of Cohesive Sediments to Water Waves, Ph.D. Dissertation, University of California, Berkeley, 149p.
- FAAS, R.A. 1995. Mudbanks of the southwest coast of India. III: Role of non-Newtonian flow properties in the generation and maintenance of mudbanks. *Journal of Coastal Research*, (in press).
- JAMES, A.E.; WILLIAMS, D.J.A., and WILLIAMS, P.R., 1988. Small strain, low shear rate rheometry of cohesive sediments. In: DRONKERS, J. and VAN LEUSSEN, W., (eds), *Physical Processes in Estuaries*. Berlin: Springer-Verlag, pp. 488-500.
- JIANG, F. 1993. Bottom Mud Transport Due to Water Waves, Ph.D. Dissertation, University of Florida, Gainesville, 222p.
- JIANG, F. and MEHTA, A.J., 1992. Some observations on fluid mud response to water waves, In: PRANDLE, D. (ed), *Dynamics and Exchanges in Estuaries and the Coastal Zone*. Washington, DC: American Geophysical Union, pp. 351-376.
- JIANG, F. and MEHTA, A.J., 1993. Some observations on water wave attenuation over nearshore underwater mudbanks and mud berms, *Report UFL/COEL/MP-93/01*, Coastal and Oceanographic Engineering Department, University of Florida, Gainesville, 45p.
- KEDDWELL, M.J. 1984. *Rheology and Soil Mechanics*, London: Elsevier, 339p.
- KOLSKY, H. 1992. The measurement of material damping of high polymers over ten decades of frequency and its interpretation, In: KINRA, V.K. and WOLFENDEN, A. (eds), *Mechanics and Mechanisms of Material Damping*. Philadelphia, PA: ASTM Publications, pp. 4-27.
- KRIZEK, R.J. 1971. Rheological behavior of clay soils subjected to dynamic loads. *Transactions of the Society of Rheology*, 15(3), 433-489.
- MAA, P.-Y. 1986. Erosion of Soft Mud by Waves, Ph.D. Dissertation, University of Florida, Gainesville, 296p.
- MALVERN, L.E. 1969. *Introduction to the Mechanics of a Continuous Medium*, Englewood Cliffs: Prentice-Hall, New Jersey, 713p.
- MATHEW, J.; BABA, M., and KURIAN, N.P., 1994. Mudbanks of the southwest coast of India. I: Wave characteristics. *Journal of Coastal Research*, (in press).
- SCHREUDER, F.W.A.M.; VAN DIEMAN, A.J.G., and STEIN, H.N., 1986. Viscoelastic properties of concentrated suspensions. *Journal of Colloid and Interface Science*, 111(1), 35-43.
- WELLS, J.T. and KEMP, G.P., 1986. Interaction of surface waves and cohesive sediments: field observations and geologic significance. In: MEHTA, A.J. (ed.), *Estuarine Cohesive Sediment Transport*. Berlin: Springer-Verlag, pp. 43-65.
- WILLIAMS, D.J.A. and WILLIAMS, P.R., 1992. Laboratory experiments on cohesive soil bed fluidization by water waves, part II, *in situ* rheometry for determining the dynamic response of bed. *Report UFL/COEL-92/015*, Coastal and Oceanographic Engineering Department, University of Florida, Gainesville, 24p.